Chemical pressure driven orthorhombic distortion and significant enhancement of ferroelectric polarization in $Ca_{1-x}La_xBaCo_4O_7$ ($x \leq 0.05$)

K. Dey[1], A. Indra[1], A. Chatterjee[1], S. Majumdar[1], U. Rütt[2], O. Gutowski[2], M. v. Zimmermann[2], and S. Giri[1]
[1]*Department of Solid State Physics, Indian Association for the Cultivation of Science, Jadavpur, Kolkata 700032, India and*
[2]*Deutsches Elektronen-Synchrotron DESY, Notkestr. 85, 22603 Hamburg, Germany*

We report significant correlation of the multiferroic order and ferroelectric polarization to the orthorhombic structural distortion for $Ca_{1-x}La_xBaCo_4O_7$ ($x \leq 0.05$). Analysis of the synchrotron diffraction studies reveal that La doping increases considerable structural distortion, which is associated with the increase of multiferroic ordering temperature and electric polarization. Intriguingly, the value of polarization increases remarkably to $\approx 385\mu C/m^2$ ($x = 0.05$) from $\approx 150\mu C/m^2$ ($x = 0$) for a 3 kV/cm poling field. Synchrotron diffraction studies in magnetic field provides an important clue, where structural distortion provides more impact on the polarization value than the contribution from the change in unit cell volume. Geometric magnetic frustration holds the key for the occurrence of the structural distortions, around which multiferroic ordering takes place for $CaBaCo_4O_7$. Our work thus highlights crystal structural distortion as a rich playground for tuning multiferroic order as well as polarization value.

PACS numbers: 75.80.+q, 77.80.-e

I. INTRODUCTION

Geometric frustration is one of the key issues in magnetism, which directs the magnetic ground state of the system, leading various rich consequences such as spin glasses,[1] spin ice,[2,3] spin liquid states.[4] Concept of frustration starts from the nearest neighboring antiferromagnetic interaction, in which frustration usually occurs due to the simplified geometric units. These are usually two dimensional triangular, kagomé, and three dimensional pyrochlore lattices.[1] In few occasions magnetic frustration is released by a strong structural distortion, which leads to the breaking of space inversion symmetry and ferroelectricity appears.[5–7] Ferroelectricity has also been observed in the geometrically frustrated systems, where noncentrosymmetry involves non-collinear spiral spin order as observed in $TbMnO_3$,[8] nickelates $Ni_3V_2O_8$,[9] delafossites $CuFeO_2$,[10] rocksalt $ACrO_2$,[11,12] spinel ACr_2X_4.[7,13–16]

Recently, the 114 cobaltite $CaBaCo_4O_7$ (CBCO) attracts special attention for intricate geometrically frustrated network as shown in Fig. 1. As addressed by the neutron powder diffraction studies,[17] CBCO forms alternate stacking of two dimensional triangular (T) lattice composed of Co1 atom and kagomé (K) lattice composed of Co2, Co3, and Co4 atoms, providing significant magnetic frustration. The CBCO consists of CoO_4 tetrahedral network fitted in a noncentrosymmetric $Pbn2_1$ space group over a wide temperature range 4-293 K with c axis as a polar axis.[17,18] Magnetization results indicated a paramagnetic to ferrimagnetic transition around $\sim$ 62 K associated with an extraordinary large coercivity of $\sim$ 20 kOe at 5 K.[19] Although CBCO crystallized in a polar $Pbn2_1$ space group close to room temperature, ferroelectric (FE) order (T_C) was reported at T_N, pointing an improper ferroelectricity.[20] In the single crystalline CBCO a considerable magnetoelectric (ME) effect was observed, which was found maximum just below FE T_C along c axis.[21] The magnetic $m'm2'$ Heesch-Schubnikov point group was proposed for the coexistence of improper ferroelectricity and ferrimagnetism in CBCO.[20,21] In accordance with the experimental evidence, the *first principles* density functional calculations proposed that the strong orthorhombic distortion of the structure weakened the geometrical frustration and established ferrimagnetic order.[22] In order to address colossal ME coupling, the *ab intio* calculations revealed that exchange striction was accountable for producing a giant change in electric polarization.[23] Further calculations using Landau theory proposed that magnetoelastic consequence in CBCO was correlated to the strong ME coupling.[23] This compound has been revisited theoretically and experimentally focusing different aspects of magnetism, ferroelectricity, and magnetoelectric coupling. Significantly, the role of structural correlations to the ferrimagnetic, ferroelectric ordering, and magnetoelectric coupling were always addressed in CBCO, although experimental evidences of which were missing in detail.

Structural correlations to the ferroelectric order were recently addressed in various films. Tuning of ferroelectric property driven by the epitaxial strain has been recently studied in $TbMnO_3$,[24] $BaTiO_3$,[25] and $BiFeO_3$ films.[26,27] In contrast, the investigations on $BiFeO_3$[28] and $PbZr_{0.2}Ti_{0.8}O_3$[29] films did not reveal any strain dependent change in the electric polarization. The magnetoelastic couplings were found responsible for the largest polarization in bulk perovskite systems, as addressed from the *first principles* calculations.[30] The influence of structural distortion revealed in polycrystalline $ABi_2Ta_2O_9$ (A = Ca, Sr, and Ba), which leaded to the higher Curie temperature and larger spontaneous ferroelectric polarization.[31] In this study structural distortions are investigated from the synchrotron diffraction studies, where distortions are systematically found to be associated with the significant increase of electric polarization

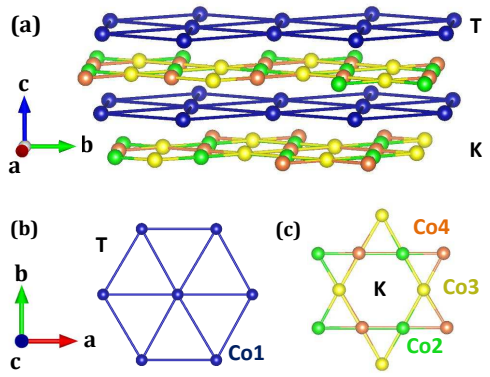

FIG. 1. (Color online) (a) Alternate arrangements of triangular (T) layer composed of Co1 and kagomé (K) layer composed of Co2, Co3, and Co3 atoms. (b) T lattice and (c) corner sharing K lattice in the $a-b$ plane.

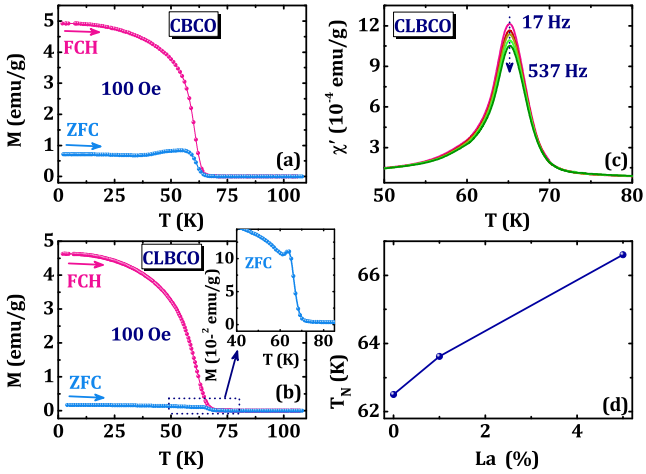

FIG. 2. (Color online) Thermal (T) variations of ZFC-FC magnetization for CBCO (a) and CLBCO (b). Inset of (b) highlights the transition region. (c) T variation of real component of ac susceptibility (χ') in the frequency (f) range, 17−537 Hz. (d) Variation of Néel temperature (T_N) with La doping (x).

and ferroelectric Curie temperature. In addition to the ferroelectric ordering, structural distortion is also found to be correlated to the magnetic ordering. Interplay between long range magnetic ordering, geometric magnetic frustration, and structural distortion are discussed in this study.

Till date, CBCO holds the largest orthorhombic distortion in 114 type RBaCo$_4$O$_7$ (R = rare earth) series.[21,32–35] Here, we note that the distortion is further increased by doping La^{3+} having larger ionic radius than Ca^{2+}. The enhanced structural distortion is associated with the considerable increase of electric polarization (P), FE T_C, and ferrimagnetic T_N. Intriguingly, the P value increases to $\approx 385\mu$C/m^2 due to 5 % La doping (CLBCO) from $\approx 150\mu$C/m^2 in CBCO for a 3 kV/cm poling field. A reasonable increase of P was observed below FE T_C when measurements were carried out with magnetic field.[20] The synchrotron diffraction studies with magnetic field reveal a considerable increase of unit cell volume associated with the smaller orthorhombic distortion. The results propose that anisotropic chemical pressure, occurred due to La doping, drives significant orthorhombic distortion, which efficiently manipulates the electric polarization than the influence of unit cell volume. Microscopic structural distortions around intralayer and interlayer Co atoms in T and K layers are discussed for realizing structural distortions locally from the analysis of the synchrotron diffraction studies.

II. EXPERIMENTAL DETAILS

Polycrystalline specimens, Ca$_{1-x}$La$_x$BaCo$_4$O$_7$ ($x \leq 0.05$) with x = 0, 0.01, and 0.05 are prepared by the solid state reaction.[19] The synchrotron x-ray diffraction studies are performed at P07 beam line of Petra III, Hamburg, Germany at a wavelength of 0.1252 Å (99 keV) in the temperature range, 12−300 K. A 100 kOe horizontal field magnet (Cryogenics, UK) has been employed for the high-energy x-ray diffraction studies under magnetic field. The synchrotron powder diffraction data are analyzed using Rietveld refinement with the MAUD (materials analysis using diffraction) and FullProf softwares. The pyroelectric current (I_p) is recorded at a constant temperature sweep rate using an electrometer (Keithley, model 6517B) and integrated with time for obtaining the electric polarization (P). The suitable poling electric fields are applied during the cooling process and short circuited before measurements of I_p in the warming mode. Electrical contacts are fabricated using an air drying silver paint. The dc magnetization and ac susceptibility measurements are carried out in a commercial magnetometer of Quantum Design (MPMS, evercool).

III. EXPERIMENTAL RESULTS AND DISCUSSIONS

Thermal variations of zero-field cooled (ZFC) and field-cooled (FC) magnetization recorded at 100 Oe are displayed in Figs. 2(a) and 2(b) for CBCO and CLBCO, respectively. The ZFC magnetization decreases considerably for CLBCO. The ferrimagnetic ordering is shifted to 67.5 K for CLBCO, as evident in the inset of Fig. 2(b). The values of ferrimagnetic T_N with x are depicted in Fig. 2(d). The almost linear increase of T_N with x is observed for $x \leq 0.05$. From the linear fit of inverse of susceptibility (χ^{-1}) using Curie-Weiss law we estimate paramagnetic moment, $\mu_{eff} \approx 4.3$, 4.2, and 3.8 μ_B for x = 0, 0.01, and 0.05, respectively. The values of μ_{eff} decrease systematically with increasing x, indicating that replacement of Ca^{2+} with La^{3+} causes partial conversion

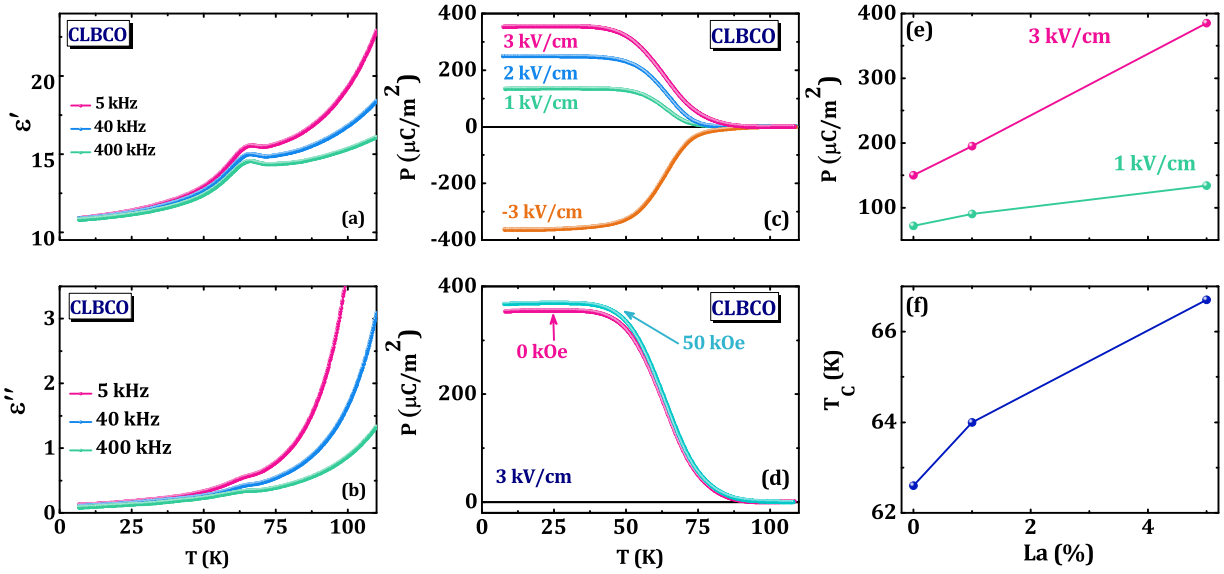

FIG. 3. (Color online) Thermal (T) variations of (a) ϵ', (b) ϵ'' at different f, (c) electric polarization (P) at different poling fields, (d) P with T at $E = 3$ kV/cm in zero field and field ($H = 50$ kOe). Variations of (e) P at two poling fields and (f) FE T_C with percentage of La doping.

of Co ion valency from Co^{3+} to Co^{2+}. The large values of Θ/T_N ratio ~ 32.3, 30.0, and 26.6 for $x = 0$, 0.01, and 0.05, respectively point to the strong magnetic frustration, which slowly decreases with increasing La doping. In order to address possible glassy magnetic behavior for CLBCO, the ac susceptibility data is recorded at different frequencies around 66.7 K, as shown in Fig. 2(c). Any convincing frequency dependent shift of the peak is absent at T_N, signifying the absence of a glassy magnetic component.

The dielectric permittivity (ϵ) is measured around T_N at different frequencies (f). The real (ϵ') and imaginary (ϵ'') components are depicted with temperature at selective f in Figs. 3(a) and 3(b), respectively. An evident signature of maximum is observed at T_N for both $\epsilon'(T)$ and $\epsilon''(T)$, pointing magnetoelectric coupling. The peak position does not change with f. This indicates occurrence of a long range ferroelectric order close to T_N. To confirm the ferroelectric order, I_p is recorded with T at different conditions for three compounds with $x = 0$, 0.01, and 0.05. A peak in $I_p(T)$ is observed in all the cases. The $I_p(T)$ is recorded at different heating rates for a particular poling field and time integrated I_p for different heating rates provides a single polarization curve as a function of T. The value of $P(T)$ for CBCO is found consistent with the previous reports.[20,21] Here, the $P(T)$ for CLBCO are depicted in Fig. 3(c) for different poling fields. Electric polarization reverses for negative poling field, pointing occurrence of the ferroelectricity. The value of P increases with increasing poling field up to 3 kV/cm, indicating that it does not saturate around 3 kV/cm. Importantly, the value of P raises to $\approx 385\mu C/m^2$ with a 5 % La doping for CLBCO from $\approx 150\mu C/m^2$ for CBCO, as shown in Fig. 3(e) for 3 kV/cm poling field. The results are also associated with the increase of T_C due to La doping, as shown in Fig. 3(f). The systematic increase of P value and FE T_C are strongly correlated to the orthorhombic structural distortion, as addressed below during discussions of the structural properties. As depicted in Fig. 3(d), the $P(T)$ increases moderately upon application of 50 kOe magnetic field below T_C, pointing the magnetoelectric coupling for CLBCO.

The synchrotron diffraction studies are performed over a wide temperature range of 12−300 K. Diffraction patterns of all three compounds ($x = 0$, 0.01, and 0.05) at 300 K are depicted in Fig. 4(a). A selected 2θ regime is highlighted in the inset of Fig. 4(a). Figure 4(b) shows the diffraction patterns at three selective temperatures (10, 50, and 100 K). Inset of the figure highlights the changes of the peak shape in a selected 2θ region above, below, and around the multiferroic ordering temperature. Lattice parameters are obtained from the careful analysis of the diffraction patterns using Rietveld refinement. The refinements of the diffraction patterns of all three samples are done using an orthorhombic $Pbn2_1$ symmetry at 300 K. Synchrotron diffraction studies and the refinements in the entire temperature range are also done using the same $Pbn2_1$ space group for CBCO and CLBCO. Examples of reasonably good refinements of the diffraction patterns at 20 K are displayed in Figs. 4(c) and 4(d) for CBCO and CLBCO, respectively. Insets of the figures show the refinement in a small 2θ range and authenticate good fit of the diffraction patterns with the small reliability parameters $R_w(\sim 4.31)$, $R_{\rm exp}(\sim 1.51)$, and $\chi^2(\sim 2.10)$ for CBCO and $R_w(\sim 4.40)$, $R_{\rm exp}(\sim 1.47)$, and $\chi^2(\sim 2.98)$

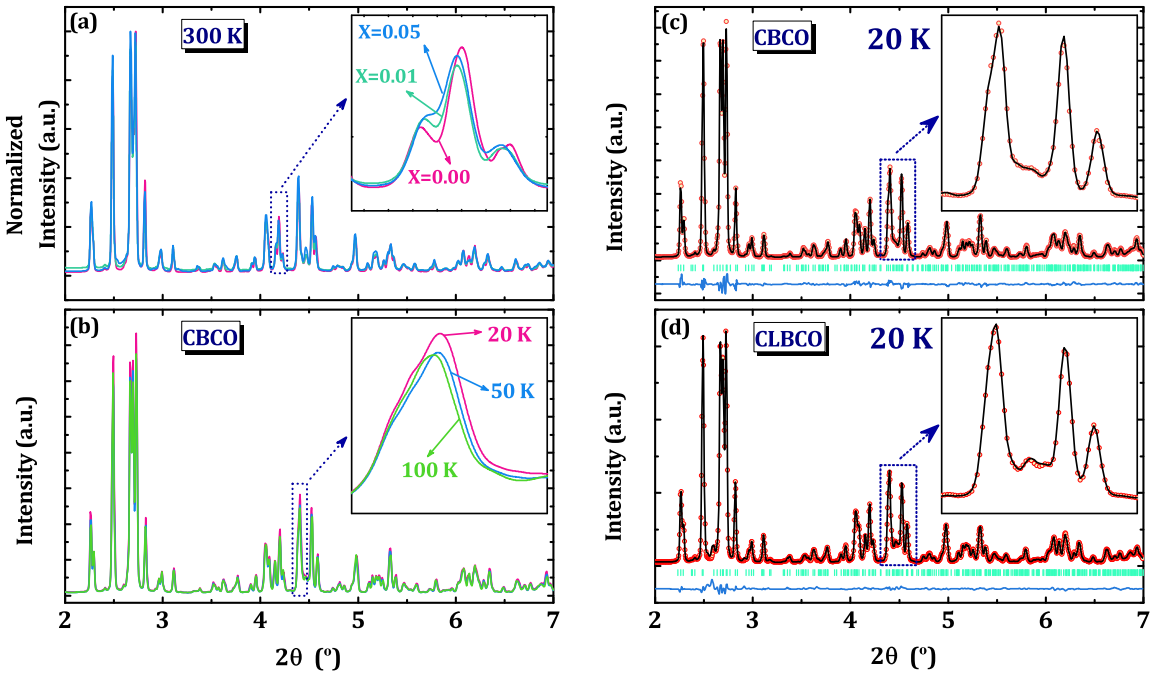

FIG. 4. (Color online) (a) Synchrotron diffraction patterns at 300 K for $x = 0$, 0.01, and 0.05 of $Ca_{1-x}La_xBaCo_4O_7$. Inset highlights modification of the pattern in a small 2θ region. (b) Diffraction patterns of $x = 0$ at three selective temperatures at 20, 50, and 100 K. Inset highlights the changes with temperature in a small 2θ region. Rietveld refinements of the pattern of (c) CBCO and (d) CLBCO at 20 K. Insets show satisfactory fits in a small 2θ region.

for CLBCO. The difference plots shown at the bottom confirm single phase without trace amount of impurity.

Thermal variations of lattice parameters, a, b, and c, as obtained from the refinements, are depicted in Figs. 5(a-c) and Figs. 5(e-g) for CBCO and CLBCO, respectively. The lattice parameters of CBCO are consistent with the reported results, as obtained from the neutron diffraction studies.[21] Here, we are interested in the structural results in the low temperature regime around multiferroic ordering, which is missing so far. So structural results with small interval in the temperature variation are given in Fig. 5 for the range of 12−110 K. The a and b parameters increase below FE T_C for CBCO and display a maximum, followed by a decrease below $\sim$ 25 K for CBCO. Notably, the largest magnetodielectric response was observed in CBCO below FE T_C, at which the a parameter exhibits a maximum in the current investigation.[20] The c decreases with decreasing temperature and the decreasing trend becomes faster below T_C or T_N. Significant decrease of c suggests that interlayer (T and K layers) distance decreases, which directs gradually stronger interlayer coupling with decreasing T below T_N. The evident signature of T_N in the lattice constants suggests strong magnetoelastic coupling. The maximum values of anomalous increases of a and b from the corresponding values at T_C are remarkable as $\sim$ 0.08 and $\sim$ 0.03 %, respectively for CBCO. This also leads to the anomalous increase of unit cell volume just below T_C, as evident in Fig. 5(d). All these features in lattice constants and unit cell volume smear out in CLBCO as shown in Figs. 5(e-h). Unit cell volume increases to $\sim$ 0.2 % due to 5 % La doping. It is important to note that CBCO has been proposed to show largest orthorhombic distortion in 114 type $RBaCo_4O_7$ (R = rare earth) series.[21,32–35] The orthorhombic distortion is quantified as $D = (b/\sqrt{3} - a)/a$. The values of D normalized by the D value at 115 K against T are shown in Fig. 6 for CBCO and CLBCO. The normalized D values, indicative of the orthorhombic distortion, deviate from each other below $\sim$ 87 K, where the difference increases systematically with decreasing temperature. Significantly, the values of normalized D are always larger for CLBCO than the values of CBCO below $\sim$ 87 K. This clearly demonstrates that orthorhombic distortion enhances further due to La doping. The enhanced distortion causes lifting of geometric magnetic frustration of CLBCO at a higher temperature than CBCO and ferrimagnetic ordering of CLBCO shifts toward the higher temperature.

The release of geometric magnetic frustration and occurrence of structural distortion are the correlated phenomena. Here, two kinds of geometric frustrations are observed in T and K layers, as described in Fig. 1. Thus displacements of Co atoms forming triangular and kagomé lattices need to be probed microscopically for realizing distortions locally. From the positional coordinates of Co atom, as obtained from the Rietveld re-

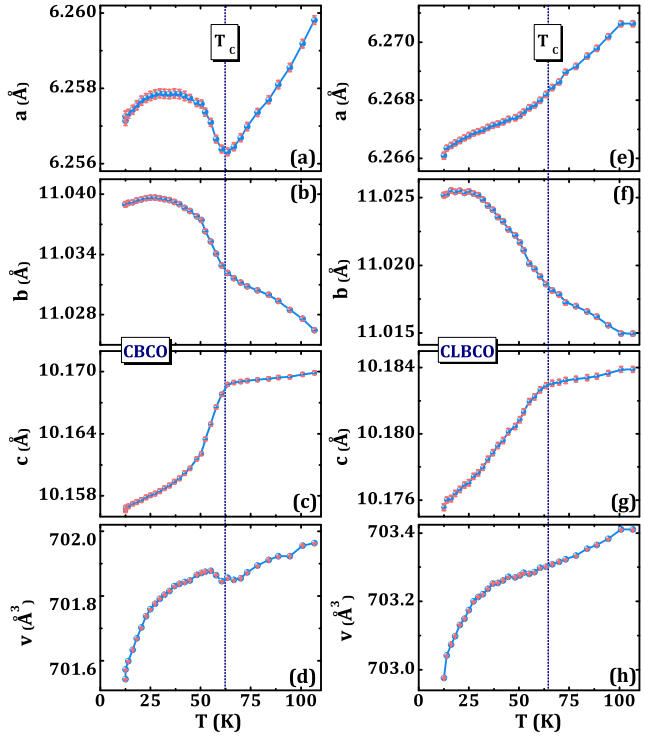

FIG. 5. (Color online) Thermal (T) variations of lattice parameters, (a) a, (b) b, (c) c, and (d) unit celle volume v for CBCO and (e) a, (f) b, (g) c, and (h) v for CLBCO. Vertical broken lines show corresponding FE T_Cs.

finements, we note that the average interatomic distance within Co1 atoms forming triangular lattice in T layer is comparable to the doubled of the average interatomic distance between Co2, Co3, and Co4 atoms forming the kagomé lattice in K layer. This indicates that T layer magnetic frustration is much weaker than the K layer magnetic frustration. Thus distortions within kagomé lattice and interlayer distortions between Co1 atom in T layer and K layer atoms (Co2, Co3, and Co4) are investigated for both CBCO and CLBCO.

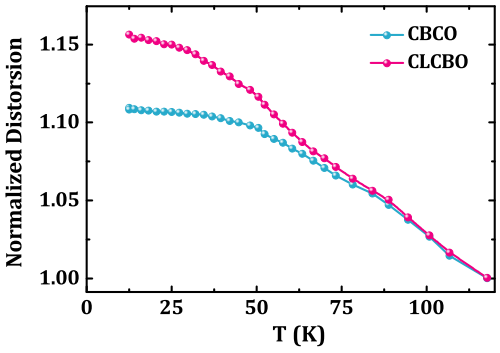

FIG. 6. (Color online) Distortion parameters normalized by the values at 115 K with T for CBCO and CLBCO.

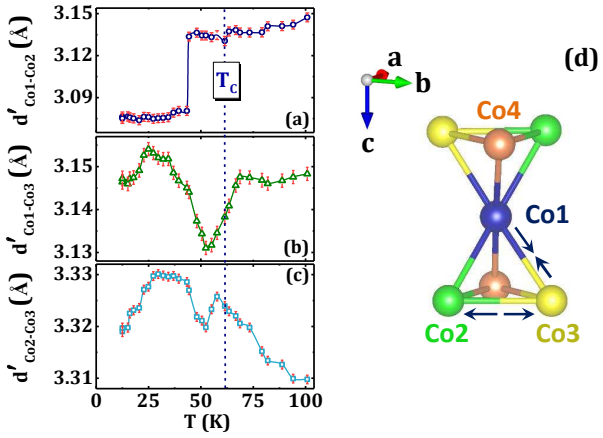

FIG. 7. (Color online) For CBCO thermal (T) variations of (a) Co1−Co2 ($d'_{\mathrm{Co1-Co2}}$), (b) Co1−Co3 ($d'_{\mathrm{Co1-Co3}}$), and (c) Co2−Co3 ($d'_{\mathrm{Co2-Co3}}$) bond lengths. Vertical broken lines show the FE T_C for CBCO. (d) Local expansion of $d'_{\mathrm{Co2-Co3}}$, and contractions of $d'_{\mathrm{Co1-Co3}}$ around FE T_C.

In order to probe local structural distortions around Co atoms, all possible Co−Co bond lengths for CBCO are calculated around FE T_C. Out of all the Co-Co bond lengths, the changes around FE T_C are significant for Co1−Co2 ($d'_{\mathrm{Co1-Co2}}$), Co1−Co3 ($d'_{\mathrm{Co1-Co3}}$), and Co2−Co3 ($d'_{\mathrm{Co2-Co3}}$), which are depicted with temperature in Figs. 7(a-c) for CBCO. Here, the $d'_{\mathrm{Co1-Co2}}$ and $d'_{\mathrm{Co1-Co3}}$ represent the interlayer bond lengths whereas $d'_{\mathrm{Co2-Co3}}$ stands for the intralayer bond length. The position of the FE T_C for CBCO is shown by the broken vertical line in the figure. The apparent signature of T_C is observed in $d'_{\mathrm{Co1-Co3}}(T)$ and $d'_{\mathrm{Co2-Co3}}(T)$, which is not significant for $d'_{\mathrm{Co1-Co2}}(T)$. We note that the changes from 90 K to the minimum in $d'_{\mathrm{Co1-Co3}}(T)$ and maximum in $d'_{\mathrm{Co2-Co3}}(T)$ are ~ 0.5 % and ~ 0.6 %, respectively. This change is negligible for $d'_{\mathrm{Co1-Co2}}(T)$ around FE T_C. The distortions around T_C are depicted in Fig. 7(d), where $d'_{\mathrm{Co1-Co3}}$ contracts and $d'_{\mathrm{Co2-Co3}}(T)$ expands around T_C. Below ~ 50 K, the $d'_{\mathrm{Co1-Co3}}(T)$ and $d'_{\mathrm{Co2-Co3}}(T)$ increase exhibiting a maximum around ~ 35 K, which is analogous to that observed similar behavior of a lattice constant below T_C, as depicted in Fig. 5(a). In contrast, a step-like fall is observed in $d'_{\mathrm{Co1-Co2}}(T)$, which is considerable as ~ 1.9 %. We note that the anomalous behavior of a lattice constant below T_C is correlated to this sharp fall in $d'_{\mathrm{Co1-Co2}}(T)$, where the anomalous increase in $a(T)$ below T_C is terminated involving this sharp considerable decrease in $d'_{\mathrm{Co1-Co2}}(T)$.

For realizing orthorhombic distortion due to La doping, the displacements of Co (Co1, Co2, Co3, and Co4) atoms are estimated with temperature around the FE T_C for CLBCO. Out of all Co−Co bond lengths, a step-like changes are observed in Co1−Co2 ($d_{\mathrm{Co1-Co2}}$), Co1−Co3 ($d_{\mathrm{Co1-Co3}}$), and Co2−Co3 ($d_{\mathrm{Co2-Co3}}$) bond lengths around FE T_C, as depicted in Fig. 8(a-c). The position of FE T_C is depicted by the broken straight

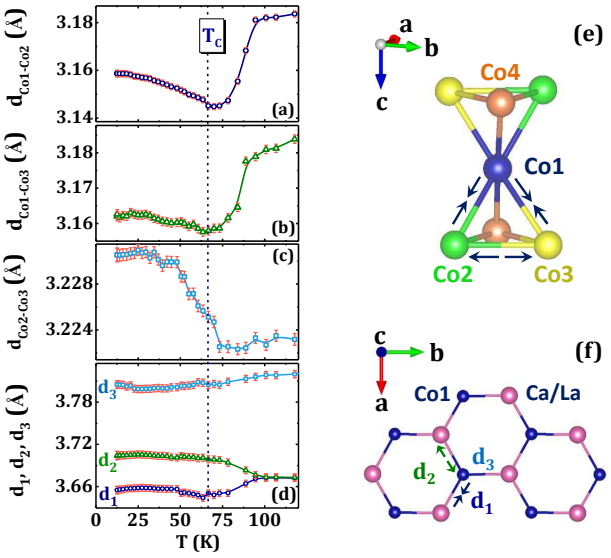

FIG. 8. (Color online) For CLBCO thermal (T) variations of (a) Co1−Co2 ($d_{\mathrm{Co1-Co2}}$), (b) Co1−Co3 ($d_{\mathrm{Co1-Co3}}$), (c) Co2−Co3 ($d_{\mathrm{Co2-Co3}}$) bond lengths, and (d) nearest neighboring Co1−Ca/La bond lengths defined as d_1, d_2, and d_3 around FE T_C. (e) Local expansion of $d_{\mathrm{Co2-Co3}}$, and contractions of $d_{\mathrm{Co1-Co2}}$ and $d_{\mathrm{Co1-Co3}}$ around FE T_C. (f) Local arrangements of Ca/La atoms in the $a-b$ plane.

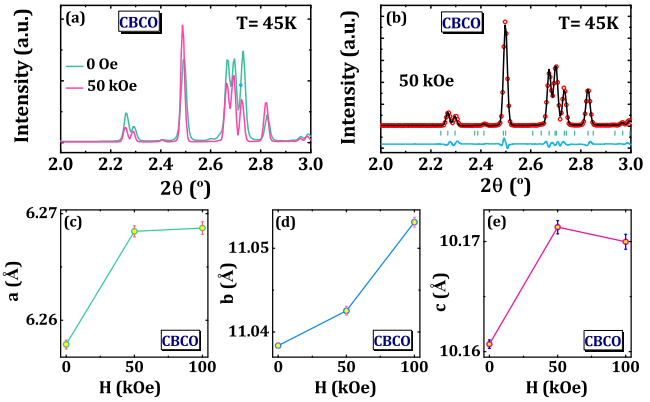

FIG. 9. (Color online) (a) Selected 2θ region of diffraction pattern at 45 K in zero field and 50 kOe. (b) Rietveld refinement of the diffraction pattern at 45 K in 50 kOe. Lattice constants, (c) a, (d) b, and (c) c with magnetic field (H) for CBCO.

lines in the figures. The changes in the bond lengths start nearly $\sim$ 20−25 K above the FE T_C, which are not evident in the lattice constants (Fig. 5). Incidentally, thermal variation of electric polarization, as evident in Fig. 3(c), exhibits that the polarization appears around 90 K, at which significant changes in the bond length start to occur. The results suggest that occurrence of structural distortion and polarization around $\sim$ 90 K is a correlated observation, where structural distortion initiates non-zero electric polarization. We further note that the changes for other bond lengths are small and almost continuous with decreasing temperature. Figure 8(e) demonstrates significant local distortions in K layer and interlayer distortions between T and K layers, where the contractions occur in $d_{\mathrm{Co1-Co2}}$ and $d_{\mathrm{Co1-Co3}}$ and expansion occurs in $d_{\mathrm{Co2-Co3}}$ around FE T_C. These changes are considerable as 1.1 %, 0.8 %, and 0.25 % for $d_{\mathrm{Co1-Co2}}$, $d_{\mathrm{Co1-Co3}}$, and $d_{\mathrm{Co2-Co3}}$, respectively. The Co−Co bond lengths around T_C exhibit different behavior due to La doping. The results for parent CBCO and La doped CLBCO show that the interlayer distortions are stronger for CLBCO than the interlayer distortions for CBCO.

In case of CLBCO, the 5 % La with larger ionic size substitutes the Ca site, where Ca occupies close to Co1 atoms residing in T layer. Arrangements of the nearest neighboring three Ca/La atoms to the Co1 atoms projected along c axis and the corresponding bond lengths are described in Fig. 8(f). Average bond lengths between three nearest neighboring Ca/La atoms to the Co1, defined as d_1, d_2, and d_3 in Fig. 8(f), are depicted with T in Fig. 8(d) around FE T_C. The d_1 and d_2 deviate from each other much above FE T_C around $\sim$ 95 K. The magnitude of d_2 increases while d_1 decreases. The changes of d_1 and d_2 are nearly same, which is $\sim$ 0.8 % around FE T_C. The d_3 decreases slowly without any evident signature around FE T_C.

It has been observed that electric polarization increases moderately when measurements were carried out with magnetic field in both the polycrystalline and single crystalline CBCO.[20,21] To test possible structural correlation to this field driven enhancement of P, we perform synchrotron diffraction studies in magnetic field (H) with 50 and 100 kOe. Diffraction patterns below FE T_C at 45 K are depicted in Fig. 9(a) in a selective 2θ region for H = 0 and 50 kOe. Diffraction patterns clearly exhibit significant modification upon application of magnetic field. Despite of significant modification in field, the diffraction patterns are satisfactorily refined with the same $Pbn2_1$ structure with the reasonably small reliability parameters $R_w(\sim 4.94)$, $R_{\mathrm{exp}}(\sim 1.69)$, and $\chi^2(\sim 2.81)$, as depicted in Fig. 9(b). Here, a small 2θ region is selected for better clarification of the fit. The refined lattice parameters are depicted with H in Figs. 9(c−e). The lattice constants, a and c increase initially and show nearly saturating trend above 50 kOe. The lattice constant, b increases systematically with increasing H. We note that unit cell volume increases to $\sim$ 0.3 % at 50 kOe, which is larger than the increase ($\sim$ 0.2 %) for 5 % La doping. Importantly, the distortion parameter does not change significantly compared to the change for the La doping. For CBCO the increase of polarization value in field was found maximum close to T_C and this increase due to application of field decreases considerably and systematically with decreasing temperature.[21] Maximum increase of P is noted to be $\sim$ 1.09 times for the measurement at 50 kOe,[20] which is

much smaller than the ~ 2.5 times increase due to 5 % La doping. Current investigation confirms that anisotropic chemical pressure driven additional orthorhombic distortion strongly influences on the increase of polarization compared to the influence of unit cell volume driven by the application of magnetic field.

IV. SUMMARY AND CONCLUSION

Our studies reveal coexistence of geometric magnetic frustration and orthorhombic structural distortions, where distortion driven multiferroic order occurs as a result of release of magnetic frustration in $CaBaCo_4O_7$. The influence of Ca doping by La is investigated on $Ca_{1-x}La_xBaCo_4O_7$ ($x \leq 0.05$). Rietveld refinements of the synchrotron diffraction studies reveal significant increase of orthorhombic structural distortion due to La doping. Interlayer distortion is identified stronger for La doped CLBCO than the parent CBCO compound. Intriguingly, additional orthorhombic distortion driven by the La doping causes considerable enhancement of polarization value and reasonable increase of multiferroic ordering temperature. Magnetic field driven structural changes are observed, which involves considerable increase of unit cell volume associated with the small change in distortion parameter. Overall results identify that engineering of structural distortion driven by the anisotropic chemical pressure directs efficient tuning of polarization and manipulation of multiferroic order toward higher temperature, which are promising and attracts the community.

Acknowledgment
S.G. acknowledges the financial support from the SERB project (Project No.: SB/S2/CMP-029/2014) and support for the synchrotron diffraction experiments at DESY, Germany under DST-DESY project (Proposal no.: I-20130286).

[1] A. P. Ramirez, Annu. Rev. Mater. Sci. **24**, 453 (1994).
[2] Steven T. Bramwell and Michel J. P. Gingras, Science **294**, 1495 (2001).
[3] R. F. Wang, C. Nisoli, R. S. Freitas, J. Li, W. McConville, B. J. Cooley, M. S. Lund, N. Samarth, C. Leighton, V. H. Crespi, and P. Schiffer, Nature Nature **439**, 303 (2005).
[4] L. Balents, Nature **464**, 199 (2010).
[5] H. D. Zhou, L. L. Lumata, P. L. Kuhns, A. P. Reyes, E. S. Choi, N. S. Dalal, J. Lu, Y. J. Jo, L. Balicas, J. S. Brooks, and C. R. Wiebe, Chem. Mater. **21**, 156 (2009).
[6] X. Fabréges, S. Petit, I. Mirebeau, S. Pailhés, L. Pinsard, A. Forget, M. T. Fernandez-Diaz, and F. Porcher, Phys. Rev. Lett. **103**, 067204 (2009).
[7] K. Dey, S. Majumdar, and S. Giri, Phys. Rev. B **90**, 184424 (2014).
[8] T. Kimura, T. Goto, H. Shintani, K. Ishizaka, T. Arima, Y. Tokura, Nature **426**, 55 (2003).
[9] G. Lawes, A. B. Harris, T. Kimura, N. Rogado, R. J. Cava, A. Aharony, O. Entin-Wohlman, T. Yildirim, M. Kenzelmann, C. Broholm, and A. P. Ramirez, Phys. Rev. Lett. **95**, 087205 (2005).
[10] T. Kimura, J. C. Lashley, and A. P. Ramirez, Phys. Rev. B **73**, 220401(R) (2006).
[11] S. Seki, Y. Onose, and Y. Tokura, Phys. Rev. Lett. **101**, 067204 (2008).
[12] K. Dey, A. Karmakar, S. Majumdar, and S. Giri, Phys. Rev. B **87**, 094403 (2013).
[13] Y. Yamasaki, S. Miyasaka, Y. Kaneko, J.-P. He, T. Arima, and Y. Tokura, Phys. Rev. Lett. **96**, 207204 (2006).
[14] J. Hemberger, P. Lunkenheimer, R. Fichtl, H.-A. Krug von Nidda, V. Tsurkan, and A. Loidl, Nature **434**, 364 (2005).
[15] L. Lin, H. X. Zhu, X. M. Jiang, K. F. Wang, S. Dong, Z. B. Yan, Z. R. Yang, J. G. Wan, and J.-M. Liu, Sci. Rep. **4**, 6530 (2015).
[16] K. Dey, A. Karmakar, A. Indra, S. Majumdar, U. Rütt, O. Gutowski, M. v. Zimmermann, and S. Giri, Phys. Rev. B **92** , 024401 (2015).
[17] V. Caignaert, V. Pralong, V. Hardy, C. Ritter, and B. Raveau, Phys. Rev. B **81**, 094417 (2010).
[18] M. Valldor and M Andersson, Solid State Sci. **4**, 923 (2002).
[19] V. Caignaert, V. Pralong, A. Maignan, and B. Raveau, Solid State Commun. **149**, 453 (2009).
[20] K. Singh, V. Caignaert, L. C. Chapon, V. Pralong, B. Raveau, and A. Maignan, Phys. Rev. B **86**, 024410 (2012).
[21] V. Caignaert, A. Maignan, K. Singh, Ch. Simon, V. Pralong, B. Raveau, J. F. Mitchell, H. Zheng, A. Huq, and L. C. Chapon, Phys. Rev. B **88**, 174403 (2013).
[22] S. Chatterjee and T. Saha-Dasgupta, Phys. Rev. B **84**, 085116 (2011).
[23] R. D. Johnson, K. Cao, F. Giustino, and P. G. Radaelli, Phys. Rev. B **90**, 045129 (2014).
[24] K. Shimamoto, S. Mukherjee, S. Manz, J. S. White, M. Trassin, M. Kenzelmann, L. Chapon, T. Lippert, M. Fiebig, C. W. Schneider, and C. Niedermayer, Sci. Rep. **7**, 44753 (2017).
[25] C. Dubourdieu, J. Bruley, T. M. Arruda, A. Posadas, J. Jordan-Sweet, M. M. Frank, E. Cartier, D. J. Frank, S. V. Kalinin, A. A. Demkov, and V. Narayanan, Nat. Nanotech. **8**, 748 (2013).
[26] H.-J. Liu, C.-W. Liang, W.-I Liang, H.-J. Chen, J.-C. Yang, C.-Y. Peng, G.-F. Wang, F.-N. Chu, Y.-C. Chen, H.-Y. Lee, L. Chang, S.-J. Lin, and Y.-H. Chu, Phys. Rev. B **85**, 014104 (2012).
[27] C. Daumont, W. Ren, I. C. Infante, S. Lisenkov, J. Allibe, C. Carrétéro, S. Fusil, E. Jacquet, T. Bouvet, F. Bouamrane, S. Prosandeev, G. Geneste, B. Dkhil, L. Bellaiche, A. Barthélémy, and M. Bibes, J. Phys.: Condens. Mater **24**, 162202 (2012).
[28] D. H. Kim, H. N. Lee, M. D. Biegalski, and H. M. Christen, Appl. Phys. Lett. **92**, 012911 (2008).

[29] H. N. Lee, S. M. Nakhmanson, M. F. Chisholm, H. M. Christen, K. M. Rabe, and D. Vanderbilt, Phys. Rev. Lett. **98**, 217602 (2007).
[30] H. J. Zhao, L. Bellaiche, X. M. Chen, and J. Íñiguez, Nat. Commun. **8**, 14025 (2017).
[31] Y. Shimakawa, Y. Kubo, Y. Nakagawa, S. Goto, T. Kamiyama, H. Asano, and F. Izumi, Phys. Rev. B **61**, 6559 (2000).
[32] M. Valldor and M. Andersson, Solid State Sci. **4**, 923 (2002).
[33] M. Valldor, J. Phys.: Condens. Matter **16**, 9209 (2004).
[34] A. Maignan, V. Caignaert, D. Pelloquin, S. Hbert, V. Pralong, J. Hejtmanek, and D. Khomskii, Phys. Rev. B **74**, 165110 (2006).
[35] V. Caignaert, A. Maignan, V. Pralong, S. Hébert, and D. Pelloquin, Solid State Sci. **8**, 1160 (2006).